CSIAM Trans. Life Sci.
doi: 10.4208/csiam-ls.SO-2025-0001

Vol. **1**, No. 2, pp. 299-319
June 2025

Patterns of Transmission Dynamics of Severe Fever with Thrombocytopenia Syndrome Virus in Dalian: Roles of Systemic, Co-Feeding, and Transovarial Routes

Xue Zhang[1], Haotian Cui[1], Yi Zhou[2], Jun Ding[3], Kyeongah Nah[4] and Jianhong Wu[5,*]

[1] *Department of Mathematics, Northeastern University, Shenyang 110819, China.*
[2] *Dalian Municipal Center for Disease Control and Prevention, Dalian 116035, China.*
[3] *Liaoning Provincial Center for Disease Control and Prevention, Shenyang 110172, China.*
[4] *Busan Center for Medical Mathematics, National Institute for Mathematical Sciences, Busan, 49241, Republic of Korea.*
[5] *Laboratory for Industrial and Applied Mathematics, York University, Toronto, Ontario, M3J 1P3, Canada.*

Received 3 January 2025; Accepted 18 February 2025

Abstract. Severe fever with thrombocytopenia syndrome (SFTS) is an emerging tick-borne zoonotic disease caused by severe fever with thrombocytopenia syndrome virus. In recent years, there has been an increasing number of human SFTS cases in central and northeast China. In the study region, Dalian, the number of human cases in years between 2011 and 2019 exhibited recurrent patterns in synchrony with the seasonal temperature variation. Here, we develop a transmission dynamics model to incorporate contact characteristics of animal and human hosts from published literature, and fit the model to historical temperature and human incidence data in our study region to analyze trends in human SFTS incidence and the time trends of SFTS prevalence within the natural tick-host cycle. Our analysis highlights the contributions of the systemic, co-feeding, and transovarial transmission routes, and provides insights for cost-effective public health interventions targeted to reducing transmission in these coexisting transmission pathways.

AMS subject classifications: 34C25, 92D25, 92D30
Key words: SFTS, dynamics model, basic reproduction number, sensitivity analysis.

1 Introduction

Severe fever with thrombocytopenia syndrome is an emerging tick-borne zoonotic disease caused by severe fever with thrombocytopenia syndrome virus (SFTSV). Most SFTS

*Corresponding author. *Email address:* wujh@yorku.ca (J. Wu)

cases in China are distributed in rural areas of central and northeastern China, including Shandong, Hubei, Henan, Anhui, Liaoning, Zhejiang, and Jiangsu provinces. Since its first identification in the central provinces of Hubei and Henan [38] in 2009, SFTS has gradually spread to other regions of Asia, including Japan and South Korea. The primary clinical and laboratory characteristics of SFTS include fever, gastrointestinal and neurological symptoms, as well as thrombocytopenia and leukopenia, with fever being the most common symptoms. The incubation period is generally 6-14 days with an average of 9 days. The case-fatality rate ranges from 12% to 50% [13]. According to surveillance data from the China Disease Prevention and Control Information System, the incidence and prevalence of SFTS have been increasing annually [22].

Recent studies indicate that ticks are the main hosts of SFTS and play a key role in its transmission. Ticks, such as Haemaphysalis longicornis, Ixodes nipponensis, Dermacentor silvarum, and Rhipicephalus microplus, are susceptible to severe fever with thrombocytopenia syndrome virus, among which H. longicornis being the predominant tick species [14]. H. longicornis is also capable of transmitting Rickettsia japonica, Russian spring-summer encephalitis virus, and tick-borne encephalitis virus. The transmission pathways of SFTS via H. longicornis include tick bites, human-to-human contact (such as blood and bodily fluid contact), and inter-species co-feeding transmission [2,8,34]. Experimental evidence has shown that transovarial transmission is also a major source of infection in ticks [18]. The life cycle of H. longicornis consists of four stages: egg, larva, nymph, and adult, each post-egg stage requiring a different host to complete development. There are a great number of early works on stage-structured population dynamics models [3,20,32,35]. The main hosts for larvae and nymphs are rodents and birds, while adult ticks primarily feed on large mammals. In eastern China, domesticated animals H. longicornis ticks fed on include goats, cattle, pigs, deer, cats, dogs, and chickens [19]. The spread of SFTS is also influenced by environmental factors, such as climate change and land use patterns, which not only affect tick survival and activity, but also influence host behavior and distribution, thus altering the risk of transmission of SFTSV.

Early works on SFTS dynamics research mainly focused on time series forecasting. For example, Deng *et al.* [5] used a generalized additive model to study the impact of meteorological factors and tick density on SFTS transmission in Jiangsu Province, finding that temperature, wind speed, and duration of sunlight significantly increased incidence. Wang *et al.* [31] employed SARIMA, XGBoost, and LSTM models to predict the incidence trend in Hubei Province, showing that XGBoost performed well in predicting seasonal trends and monthly incidence rates. In addition, much attention is also paid to the clinical diagnosis and treatment of SFTS. Li *et al.* [15] designed a clinical scoring model, combining age and neurological symptoms with laboratory variables, including abnormal lactate dehydrogenase concentrations, aspartate aminotransferase, blood urea nitrogen, and abnormal neutrophil percentage. They further suggested the best time for the application of ribavirin. Based on hospital data collected from Henan and Shandong between 2011 and 2020, Ge *et al.* [9] compared clinical progress for patients with SFTS and acute hyperglycemia and concluded that acute hyperglycemia is responsible for SFTS-related

death in female patients. However, there have been limited studies to use disease transmission models to examine the roles of different transmission routes to inform the most effective measures for the prevention and control of SFTS, filling this gap is one of the objectives of our study.

Our transmission dynamics model will be parameterized and validated using surveillance data from the province of Liaoning. In recent years, confirmed SFTS cases have gradually increased in the southern Liaoning, mainly in Dalian. Applying descriptive analysis, joinpoint regression models, and spatial autocorrelation analysis, Qi *et al.* [24] revealed that the incidence of SFTS in Dalian shows a growing and expanding trend characterized by significant spatial clustering and distinct seasonal patterns from 2011 to 2023. Future public health interventions to be designed and used to prevent a larger outbreak of SFTS require a qualitative assessment of the contribution of transovarial, systemic, and co-feeding transmission to the spread of SFTS in the region, which we aim to provide using a novel transmission dynamics modeling framework. Future pubic health surveillance and public health messaging also requires understanding the mechanisms behind the observed/reported patterns and their variations from month to month and year to year (as our model aims to achieve), so we can develop an effective early warning system to alert the public of the incoming public infection risks and to prioritize the public health investment including the surveillance focus.

The remainder of our paper is organized as follows. In Section 2, we establish a stage-structured dynamic model for SFTS. In Section 3, we give the main procedure for data fitting. In Section 4, we estimate model parameters and calculate the basic reproduction number based on the SFTS surveillance data in the Dalian region from 2011 to 2019. Moreover, we assess the roles of different transmission routes and predict the future trend of SFTS in Dalian.

2 Modeling transmission dynamics with temperature variation

From the National Climatic Data Center (`ftp://ftp.ncdc.noaa.gov/pub/dataoaa/isd-lite/`), we downloaded the temperature data in Dalian, China. We also obtained from the Liaoning Province Center for Disease Control and Prevention the SFTS cases in the Dalian region from 2011 to 2023. We then plotted in Fig. 1 the monthly average temperature variation in the Dalian region from 2011 to 2023 (blue curve) alongside the monthly reported cases (red curve). From this figure, it follows that the seasonal trends of the temperature variation curve and the SFTS case count curve align closely, indicating that seasonal temperature changes greatly impact the development of tick populations and human activities. A study [37] also shows that temperature is a critical factor influencing ticks, and the preoviposition period, the development time from egg to larva, from larva to nymph and from nymph to adult are all temperature dependent. Therefore, in our proposed transmission dynamics model for SFTS, all relevant parameters are temperature-dependent functions.

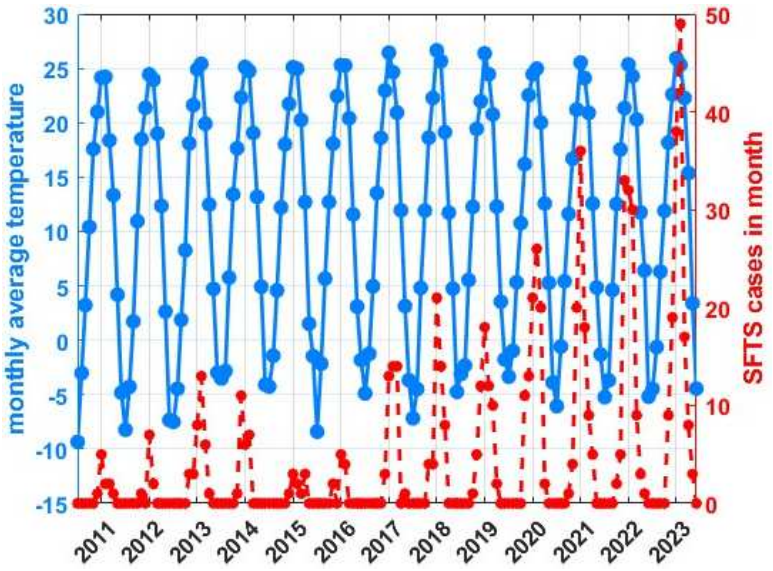

Figure 1: Average monthly temperature and reported monthly cases in Dalian region during 2011∼2023.

We start with the stratification of the main vector H. longicornis in terms of the (ecological) developmental stages and physical activities into 8 subgroups: eggs (E), questing larvae, nymphs and adults (L_q, N_q, A_q), feeding larvae, nymphs and adults (L_f, N_f, A_f), and egg-laying adults (A_l). We further divide each subgroup of H. longicornis and competent hosts by the epidemiological infection status as susceptible and infected (denoted with subscript s and i, respectively). All state variables are listed in Table 1. Our transmission dynamics model for the tick-host interaction is formulated by: 1) taking into account the dynamics of the tick population that involves the nonlinear birth process of egg-laying adults and the development of ticks by feeding on the host, 2) incorporating important pathogen transmission routes including systemic, co-feeding, and transovarial transmissions. Some outputs of the model, primarily the infected nymphs and adults,

Table 1: The state variables of the tick population.

Variable	Description	Variable	Description
E_s	Susceptible eggs	N_{fs}	Susceptible feeding nymphs
E_i	Infected eggs	N_{fi}	Infected feeding nymphs
L_{qs}	Susceptible questing larvae	A_{qs}	Susceptible questing adults
L_{qi}	Infected questing larvae	A_{qi}	Infected questing adults
L_{fs}	Susceptible feeding larvae	A_{fs}	Susceptible feeding adults
L_{fi}	Infected feeding larvae	A_{fi}	Infected feeding adults
N_{qs}	Susceptible questing nymphs	A_{ls}	Susceptible egg-laying adults
N_{qi}	Infected questing nymphs	A_{li}	Infected egg-laying adults

will be incorporated into an integration formula to account for the accumulated human cases during a particular surveillance unit.

Ecological interaction: In the Dalian region, goats are dominant hosts that H. longicornis parasitizes. Therefore, we take rodents (R) and goats (G) as principal hosts of immature and adult ticks. We consider a tick-host interaction where larvae and nymphs feed on rodents and adults on goats merely.

Epidemiological process: 1) Through the systemic transmission route, if a susceptible larva (a susceptible nymph) feeds on an infected rodent, the susceptible larva (the susceptible nymph) may be infected; and on the other hand, if an infected larva (an infected nymph) feeds on a susceptible rodent, the susceptible rodent may get infected. Similarly, systemic transmission may occur between adult ticks and goats. 2) SFTSV can also be transmitted through the co-feeding mechanism. Once a susceptible larva co-feeds on the same rodent with infected nymphs, the co-feeding transmission may take place so that the susceptible larva can acquire infection during the co-feeding period; the co-feeding transmission can also take place when a susceptible nymph (a susceptible adult) co-feeds on a rodent (a goat) with infected nymphs (infected adults). Assume that c denotes the co-feeding transmission probability that a susceptible tick acquires SFTSV through co-feeding with an infected tick on the same host. The infection probability of a susceptible tick co-feeding with j infected ticks on the same host is $1-(1-c)^j$. 3) Through transovarial transmission, SFTSV can be transmitted from an infected adult female tick to eggs.

A schematic illustration of the SFTS transmission dynamics involving three transmission routes is given in Fig. 2. The corresponding dynamics model of SFTS transmission between the tick and host population is given by the following coupled tick-host system involving ticks in four different stages and two distinct host species:

Population and transmission dynamics of eggs involving transovarial transmission:

$$\begin{aligned} E_s'(t) &= r_T d_{Legg}(t)\big(A_{ls}(t)+(1-\theta)A_{li}(t)\big)e^{-sd_{Legg}(t)A_l(t)} - d_E(t)E_s(t) - \mu_E E_s(t), \\ E_i'(t) &= r_T d_{Legg}(t)\theta A_{li}(t)e^{-sd_{Legg}(t)A_l(t)} - d_E(t)E_i(t) - \mu_E E_i(t). \end{aligned} \tag{2.1}$$

Population and transmission dynamics of larvae involving systemic and co-feeding transmission:

$$\begin{aligned} L_{qs}'(t) &= d_E(t)E_s(t) - \beta_{L_q}(t)L_{qs}(t) - \mu_{L_q}L_{qs}(t), \\ L_{qi}'(t) &= d_E(t)E_i(t) - \beta_{L_q}(t)L_{qi}(t) - \mu_{L_q}L_{qi}(t), \\ L_{fs}'(t) &= \big(1-\eta_{NL}(t)\big)\frac{R_s(t)}{R(t)}\beta_{L_q}(t)L_{qs}(t) + \big(1-\eta_{NL}(t)\big)(1-p_{RL})\frac{R_i(t)}{R(t)}\beta_{L_q}(t)L_{qs}(t) \\ &\quad - d_{L_f}(t)L_{fs}(t) - \mu_{L_f}L_{fs}(t), \\ L_{fi}'(t) &= \eta_{NL}(t)\frac{R_s(t)}{R(t)}\beta_{L_q}(t)L_{qs}(t) + p_{RL}\frac{R_i(t)}{R(t)}\beta_{L_q}(t)L_{qs}(t) \\ &\quad + \eta_{NL}(t)(1-p_{RL})\frac{R_i(t)}{R(t)}\beta_{L_q}(t)L_{qs}(t) + \beta_{Lq}(t)L_{qi}(t) - d_{L_f}(t)L_{fi}(t) - \mu_{L_f}L_{fi}(t). \end{aligned} \tag{2.2}$$

Population and transmission dynamics of nymphs involving systemic and co-feeding transmission:

$$\begin{aligned}
N'_{qs}(t) &= d_{L_f}(t)L_{fs}(t) - \beta_{N_q}(t)N_{qs}(t) - \mu_{N_q}N_{qs}(t),\\
N'_{qi}(t) &= d_{L_f}(t)L_{fi}(t) - \beta_{N_q}(t)N_{qi}(t) - \mu_{N_q}N_{qi}(t),\\
N'_{fs}(t) &= \big(1-\eta_{NN}(t)\big)\frac{R_s(t)}{R(t)}\beta_{N_q}(t)N_{qs}(t) + \big(1-\eta_{NN}(t)\big)(1-p_{RN})\frac{R_i(t)}{R(t)}\beta_{N_q}(t)N_{qs}(t)\\
&\quad - d_{N_f}(t)N_{fs}(t) - \mu_{N_f}N_{fs}(t),\\
N'_{fi}(t) &= p_{RN}\frac{R_i(t)}{R(t)}\beta_{N_q}(t)N_{qs}(t) + \eta_{NN}(t)\frac{R_s(t)}{R(t)}\beta_{N_q}(t)N_{qs}(t)\\
&\quad + \eta_{NN}(t)(1-p_{RN})\frac{R_i(t)}{R(t)}\beta_{N_q}(t)N_{qs}(t) + \beta_{N_q}(t)N_{qi}(t)\\
&\quad - d_{N_f}(t)N_{fi}(t) - \mu_{N_f}N_{fi}(t).
\end{aligned} \tag{2.3}$$

Population and transmission dynamics of adults involving systemic and co-feeding transmission:

$$\begin{aligned}
A'_{qs}(t) &= d_{N_f}(t)N_{fs}(t) - \beta_{A_q}(t)A_{qs}(t) - \mu_{A_q}A_{qs}(t),\\
A'_{qi}(t) &= d_{N_f}(t)N_{fi}(t) - \beta_{A_q}(t)A_{qi}(t) - \mu_{A_q}A_{qi}(t),\\
A'_{fs}(t) &= \big(1-\eta_{AA}(t)\big)\frac{G_s(t)}{G(t)}\beta_{A_q}(t)A_{qs}(t) + \big(1-\eta_{AA}(t)\big)(1-p_{GA})\frac{G_i(t)}{G(t)}\beta_{A_q}(t)A_{qs}(t)\\
&\quad - d_{A_f}(t)A_{fs}(t) - \mu_{A_f}A_{fs}(t),\\
A'_{fi}(t) &= p_{GA}\frac{G_i(t)}{G(t)}\beta_{A_q}(t)A_{qs}(t) + \eta_{AA}(t)\frac{G_s(t)}{G(t)}\beta_{A_q}(t)A_{qs}(t)\\
&\quad + \eta_{AA}(t)(1-p_{GA})\frac{G_i(t)}{G(t)}\beta_{A_q}(t)A_{qs}(t)\\
&\quad + \beta_{A_q}(t)A_{qi}(t) - d_{A_f}(t)A_{fi}(t) - \mu_{A_f}A_{fi}(t),\\
A'_{ls}(t) &= \alpha_F d_{A_f}(t)A_{fs}(t) - d_{Legg}(t)A_{ls}(t) - \mu_{A_l}A_{ls}(t),\\
A'_{li}(t) &= \alpha_F d_{A_f}(t)A_{fi}(t) - d_{Legg}(t)A_{li}(t) - \mu_{A_l}A_{li}(t).
\end{aligned} \tag{2.4}$$

Population and transmission dynamics of hosts:

$$\begin{aligned}
R'_s(t) &= b_R\big(R(t)\big) - p_{LR}\frac{R_s(t)}{R(t)}\beta_{L_q}(t)L_{qi}(t) - p_{NR}\frac{R_s(t)}{R(t)}\beta_{N_q}(t)N_{qi}(t) - \mu_R R_s(t),\\
R'_i(t) &= p_{LR}\frac{R_s(t)}{R(t)}\beta_{L_q}(t)L_{qi}(t) + p_{NR}\frac{R_s(t)}{R(t)}\beta_{N_q}(t)N_{qi}(t) - \mu_R R_i(t),\\
G'_s(t) &= b_G\big(G(t)\big) - p_{AG}\frac{G_s(t)}{G(t)}\beta_{A_q}(t)A_{qi}(t) - \mu_G G_s(t),\\
G'_i(t) &= p_{AG}\frac{G_s(t)}{G(t)}\beta_{A_q}(t)A_{qi}(t) - \mu_G G_i(t),
\end{aligned} \tag{2.5}$$

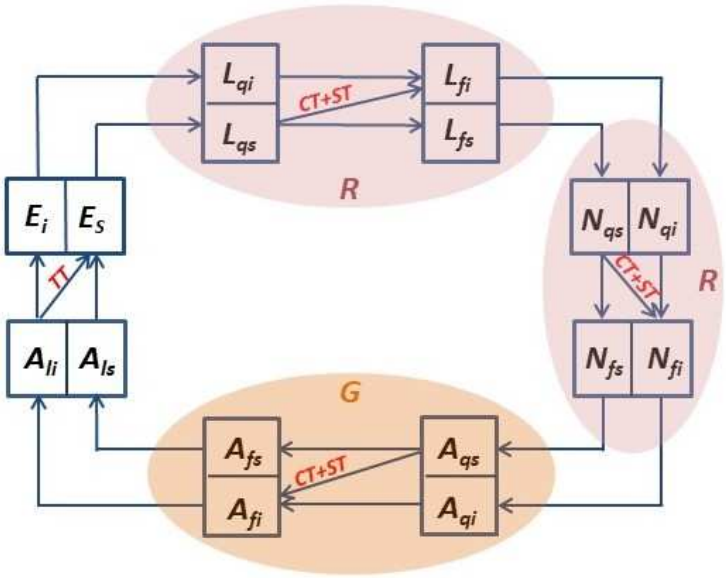

Figure 2: A schematic illustration of the SFTSV transmission dynamics involving three transmission routes: systemic transmission (ST), co-feeding transmission (CT), and transovarial transmission (TT). R and G are short for two classes of hosts, rodents and goats, respectively. Three major post-egg stages of H. longicornis are depicted by boxes on the top (larvae), the right (nymphs), and at the bottom (adults). Egg-laying ticks produce eggs and then grow into questing larvae, which are depicted through boxes on the left. There are two parallel boxes at each stage since ticks are stratified by their infectious status, and the transmission takes place when a susceptible tick takes a blood meal from an infected host (systemic transmission) or is co-fed by other infected ticks (co-feeding transmission). Egg ticks can become infected due to transovarial transmission.

where $E_s(t)$ and $E_i(t)$ represent the numbers of susceptible and infected eggs at time t, respectively; $L_{qs}(t)$ and $L_{qi}(t)$, $N_{qs}(t)$ and $N_{qi}(t)$, $A_{qs}(t)$ and $A_{qi}(t)$ denote the numbers of susceptible and infected questing ticks at larval, nymphal and adult stages at time t, respectively; $L_{fs}(t)$ and $L_{fi}(t)$, $N_{fs}(t)$ and $N_{fi}(t)$, $A_{fs}(t)$ and $A_{fi}(t)$ denote the numbers of susceptible and infected feeding ticks at larval, nymphal and adult stages at time t, respectively; $A_{ls}(t)$ and $A_{li}(t)$ are the numbers of susceptible and infected egg-laying adults, respectively; $R_s(t)$ and $R_i(t)$ are the densities of the rodents that are susceptible and infectious at time t, respectively; $G_s(t)$ and $G_i(t)$ are the densities of the goats that are susceptible and infectious at time t, respectively; $R(t)=R_s(t)+R_i(t)$ and $G(t)=G_s(t)+G_i(t)$ are the total numbers of hosts in rodents and goats, respectively; Host birth functions follow the classical logistic model

$$b_R(R)=r_R R(t)\left(1-\frac{R(t)}{K_R}\right),\quad b_G(G)=r_G G(t)\left(1-\frac{G(t)}{K_G}\right),$$

$\eta_{NL}(t)$ ($\eta_{NN}(t)$) listed in Table 2 represents co-feeding probability that a susceptible larva (or a susceptible nymph) gets co-feeding infection when it co-feeds with infected nymphs on a same rodent; $\eta_{AA}(t)$ denotes the co-feeding probability that a susceptible adult get

infection from an infected adult when they co-feed on a same goat. The descriptions of all fixed parameters and their values are listed in Tables 3 and 4, and the estimated parameters are listed in Table 5.

Table 2: The description of infectious parameters in model (2.1)-(2.5).

Parameter	Description	Value
$\eta_{NL}(N_{qi}(t),R(t))$ $(\eta_{NN}(N_{qi}(t),R(t)))$	Probability that a susceptible larva (nymph) gets non-systemic infection through co-feeding with infected nymphs on a same rodent	$1-(1-c_n)^{\frac{T_{fn}^N \beta_{Nq}(t) N_{qi}}{R(t)}}$
$\eta_{AA}(A_{qi}(t),G(t))$	Probability that a susceptible adult gets non-systemic infection through co-feeding with infected adults on a same goat	$1-(1-c_a)^{\frac{T_{fa}^A \beta_{Aq}(t) A_{qi}}{G(t)}}$

Table 3: The description of fixed parameters in model (2.1)-(2.5)-Part 1.

Parameter	Description	Value
$d_{Leeg}(t)$	Temperature-dependent proportion of egg-laying adults that can produce eggs	see the footnote below [36]
$d_E(t)$	Development rate from eggs to hardening larvae	see the footnote below [36]
$d_{L_f}(t)$	Development rate from engorged larvae to questing nymphs	see the footnote below [36]
$d_{N_f}(t)$	Development rate from engorged nymph to questing adult	see the footnote below [36]
$d_{A_f}(t)$	Development rate from engorged females to egg-laying females	see the footnote below [36]
$\beta_{Lq}(t)$	Host-attaching rate for questing larvae	$\lambda_{Lq} \times p_L(t)$ [28]
$\beta_{Nq}(t)$	Host-attaching rate for questing nymphs	$\lambda_{Nq} \times p_N(t)$ [28]
$\beta_{Aq}(t)$	Host-attaching rate for questing adults	$\lambda_{Aq} \times p_A(t)$ [28]
μ_E	Daily, per-capita mortality rate of egg	$0.002(\text{day}^{-1})$ [25]
μ_{L_q}	Daily, per-capita mortality rate of questing larvae	$0.0046(\text{day}^{-1})$ [6]
μ_{L_f}	Daily, per-capita mortality rate of feeding larvae	$0.0046(\text{day}^{-1})$ [6]
μ_{N_q}	Daily, per-capita mortality rate of questing nymph	$0.0038(\text{day}^{-1})$ [6]
μ_{N_f}	Daily, per-capita mortality rate of feeding nymph	$0.0038(\text{day}^{-1})$ [6]
μ_{A_q}	Daily, per-capita mortality rate of questing adult	$0.004(\text{day}^{-1})$ [6]
μ_{A_f}	Daily, per-capita mortality rate of feeding adult	$0.004(\text{day}^{-1})$ [6]
μ_{A_l}	Daily, per-capita mortality rate of egg-laying female	$0.34(\text{day}^{-1})$ [10]

- $d_{Leeg}(t)=\begin{cases}0, & T(t)<11.1,\\ p, & T(t)\geq 11.1,\end{cases}$
- $d_E(t)=\begin{cases}0, & T(t)<12.2,\\ -0.0391+0.00320T(t), & T(t)\geq 12.2,\end{cases}$
- $d_{L_f}(t)=\begin{cases}0, & T(t)<10.2,\\ -0.0469+0.00459T(t), & T(t)\geq 10.2,\end{cases}$
- $d_{N_f}(t)=\begin{cases}0, & T(t)<11.8,\\ -0.0506+0.00428T(t), & T(t)\geq 11.8,\end{cases}$
- $d_{A_f}(t)=\begin{cases}0, & T(t)<11.1,\\ -0.130+0.0117T(t), & T(t)\geq 11.1.\end{cases}$

Table 4: The description of fixed parameters in model (2.1)-(2.5)-Part 2.

Parameter	Description	Value
$p_i(t), i=L,N$	Temperature-dependent proportion of active questing immature ticks (larvae and nymphs)	see the footnote below [23]
$p_A(t)$	Temperature-dependent proportion of active questing adults	see the footnote below [23]
T_{fn}^N	Average duration of feeding for nymphs	3.5 days [27]
T_{fa}^A	Average duration of feeding for adult ticks	12 days [27]
α_F	Proportion of feeding female adults	0.65 [14]
r_R	Natural birth rate of rodent host	$0.14(\text{day}^{-1})$ [7]
r_G	Natural birth rate of goat host	$0.15(\text{day}^{-1})$ [1]
K_R	Carrying capacity of rodents	500 (assumed)
K_G	Carrying capacity of goat	1000 (assumed)
p_{RL} (p_{RN}, p_{LR}, p_{NR})	Probability of systemic transmission from larva(nymph) to rodent or from rodent to tick	0.5 [29]
$p_{GA}(p_{AG})$	Probability of systemic transmission from adult to goat or from goat to tick	0.7 [29]
μ_R	Natural mortality rate of rodent	$0.0277(\text{day}^{-1})$ [26]
μ_G	Natural mortality rate of goat	$0.06(\text{day}^{-1})$ [11]

- $p_L(t)=p_N(t)=\begin{cases}0, & T(t)<LN_{temp},\\ 1, & T(t)\geq LN_{temp},\end{cases}$
- $p_A(t)=\begin{cases}0, & T(t)<A_{temp},\\ 1, & T(t)\geq A_{temp}.\end{cases}$

Table 5: The description of estimated parameters in model (2.1)-(2.5).

Parameter	Description	Range
θ	Probability of infected eggs from a female egg-laying adult	$0\sim1$
p	Proportion of egg-laying adults that can produce eggs	$0\sim1$ [36]
r_T	Per-capita egg production by egg-laying females	$1000\sim2500$ [27]
s	The strength of density dependence in fecundity	$1\sim10$
c_n	Probability of an infected nymph to induce non-systemic infection to the co-feeding susceptible larva/ nymph	$0\sim1$
c_a	Probability of an infected adult to induce non-systemic infection to the co-feeding susceptible nymph	$0\sim1$
$\zeta_N(\zeta_A)$	The temperature-dependent strength on the attaching rate of nymphal and adult ticks	$0\sim0.01$
$\lambda_{Lq}(\lambda_{Nq})$	Host-seeking probability for questing larvae or nymphs	$0\sim1$
λ_{Aq}	Host-seeking probability for questing adults	$0\sim1$
LN_{temp}	Critical temperature that questing larvae(nymphs) become active	$12\sim25$ [27]
A_{temp}	Critical temperature that questing adult ticks become active	$10\sim12$ [27]
ω	The strength of human outdoor activity	$0\sim1$
E_{temp}	Critical temperature that adults that can produce eggs	$12\sim25$ [36]

Since nymphal and adult stages are the most important stages for the pathogen transmission to humans, the probability of human infection with SFTSV completely depends on the densities of questing nymphs and questing adults. The newly reported human SFTS cases during a period of duration σ take the following form:

$$\hat{y}(t)=\int_{t-\sigma}^{t}\big(\Lambda_N(s)p_N(s)N_{qi}(s)+\Lambda_A(s)p_A(s)A_{qi}(s)\big)ds, \tag{2.6}$$

where we take one month as a reporting period; $\Lambda_\Theta(s),\Theta=N,A$ are attaching rates of questing nymphs and questing adults on humans at time s, which are proportional to the temperature that impacts the human outdoor activity. Based on the literature [21], we will use

$$\Lambda_\Theta(s)=\zeta_\Theta\times e^{\omega\times T(s)},$$

where ζ_Θ, $\Theta=N,A$ represent temperature-dependent strength on the attaching rate of nymphal and adult ticks, and ω is the strength of human outdoor activity.

3 Data fitting

Generally, people infected with SFTSV do not have symptoms or get sick after an average of 10 days. The incubation period of SFTS has been reported to range from 7 to 14 days, with an average of 9 days [17]. Many patients had reported tick bites 7–9 days before

illness [33]. He *et al.* [12] compared laboratory examination results of patients in the surviving and non-surviving groups and found that 77% of patients lived in rural regions, and most of the SFTS diagnoses from symptom onset are delayed by 7 days. Hence, in the process of data fitting, we introduce τ as diagnostic delay and fix its value $\tau = 0.5$ month.

The optimum parameter values can be estimated by minimizing the sum of between the monthly estimated data and the reported one. The objective function is given as

$$f(\phi,n)=\sum_{t_n}\big(\hat{y}(t_n)-y(t_n-\tau)\big)^2,$$

where

$$\phi=(\theta,r_T,s,c_n,c_a,\lambda_{L_q},\lambda_{N_q},\lambda_{A_q},LN_{temp},A_{temp},E_{temp},\zeta_N,\zeta_A,p,\omega)$$

denotes a set containing the estimated parameters of model (2.1)-(2.5); $\hat{y}(t_n)$ is the prediction SFTS cases of the nth month following model (2.1)-(2.5) and Eq. (2.6); $y(t_n-\tau)$ is the reported cases of the $(n-\tau)$-th month. We aim to fit the model (2.1)-(2.5) and Eq. (2.6) to compare the predicted number of SFTS cases with the monthly reported data provided by Liaoning Province Center for Disease Control and Prevention. The main procedures are as follows:

(i) Specify the parameter set ϕ with appropriate random initial values listed in Table 5.

(ii) Solve model (2.1)-(2.5) numerically by using the fourth-order Runge-Kutta method.

(iii) Combine the reported SFTS data to calculate the objective function $f(\phi,n)$ based on Eq. (2.6).

(iv) Find the minimum objective function value and record the corresponding parameter set ϕ as the optimum parameter value.

4 Results

We now present our data fitting and numerical simulations to estimate the values of parameters for model (2.1)-(2.5) and investigate the effects of transovarial transmission on the spread of SFTSV in the study region.

Data Fitting and Parameter Estimation: In Fig. 3, we show the comparison of SFTS cases between the estimated (the blue line) and the reported (the red line) from 2011 to 2019 with the estimated parameters: the probability of transovarial transmission $\theta=0.072$; egg production numbers per egg-laying female $r_T=1071$; the strength of density dependence in fecundity $s=1.343$; the probability of co-feeding transmission through co-feeding on rodents and goats $c_n=0.335, c_a=0.449$; the coefficients of temperature-dependent strength on the attaching rate of nymphal and adult ticks are $\zeta_N=1.323\times10^{-9}$ and $\zeta_A=2.753\times10^{-8}$, respectively; the hosting-seeking probability for questing larvae (or nymphs) and questing adults $\lambda_{Lq}=\lambda_{Nq}=0.013, \lambda_{Aq}=0.008$; the critical temperature that questing larvae

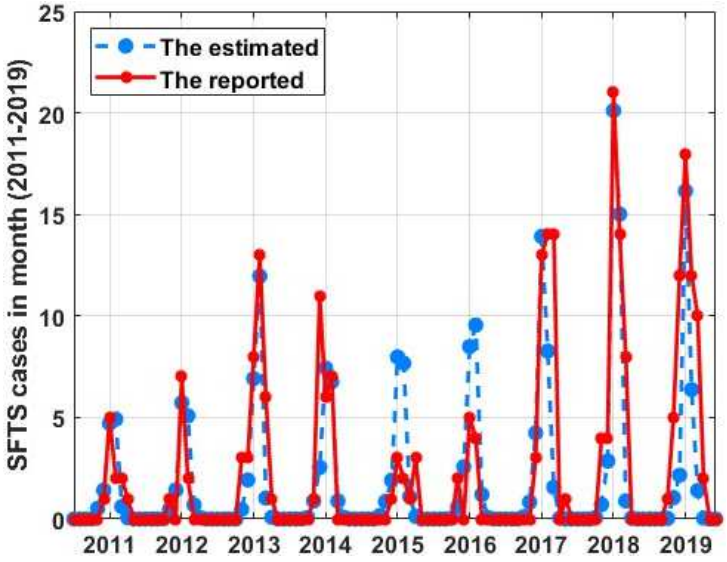

Figure 3: Monthly SFTS cases in Dalian from 2011 to 2019. The red line represents the reported cases, and the blue line represents the estimated. Using data fitting, estimated parameters are $\theta=0.072, r_T=1071, s=1.343$, c_n=0.335, c_a=0.449, ζ_N=1.323×10^{-9}, ζ_A=2.753×10^{-8}, $\lambda_{L_q}=\lambda_{N_q}$=0.013, λ_{A_q}=0.008, p=0.061, LN_{temp}=14.82, $A_{temp}=11.93, E_{temp}=13.60, \omega=0.44$, respectively.

(or nymphs) become active LN_{temp}=14.82°C; the critical temperature that questing adults become active $A_{temp}=11.93$°C; the minimal temperature adults when can produce eggs is $E_{temp}=13.60$°C; the strength of human outdoor activity $\omega=0.44$. Moreover, we also note in Fig. 3 that the monthly SFTS cases increased rapidly in 2018, directly resulting from high temperature: the highest temperature during the period 2011-2019 occurs in 2018 and reaches 31.58°C.

Validation: During the COVID-19 pandemic, daily life in the considered region returned to normal after the lockdown was lifted on April 8, 2020. Despite some temporal restrictions in specific areas due to the potential importation of COVID-19 cases, daily life in the considered region also remained normal in 2021. In 2022, the emergence of the Omicron variant triggered a lockdown that started in April, but the lockdown lasted only two months. In short, during these three years, from 2020 to 2022, the COVID-19 control restrictions were eased just before each summer, leading to a rapid rebound in summer tourism. This explains why data fitting yields the adjustment of human outdoor activity to $\omega=0.52$. Using all the values of other parameters listed in Table 5, our model gives the predicted number of SFTS cases for the years 2020-2023. The estimated and reported monthly cases are presented in Fig. 4. It should be mentioned that in Fig. 4, the maximum values of the estimated monthly SFTS cases for the three years (2020-2022) are in strong alignment with the reported values. However, the model-based estimate is clearly an underestimate of the reported value in 2023, and this is anticipated since in 2023, China officially ended the dynamic zero COVID policy, and tourism increased sig-

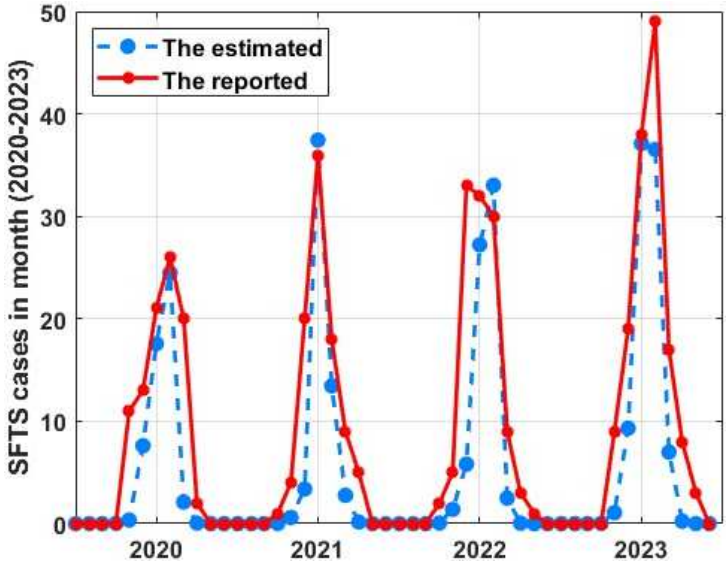

Figure 4: The comparison of monthly SFTS cases during 2020-2023 based on the estimated parameters listed in Table 5.

nificantly, leading to increased human outdoor activity. Moreover, we compare the total SFTS cases per year from 2020 to 2022 with the number in 2023. The effect of lockdown is a decrease in the risk of acquiring SFTS infection up to 29.8%.

Basic Reproduction Number and Contributions of Three Transmission Routes: H. longicornis completes its life cycle in six months, with one generation occurring yearly [16]. Therefore, we can treat the model as a periodic system with period $1-$ year with varying temperature conditions within a given year to calculate the basic reproduction number for each year $R_0^{(201i)}$ $(i=1,2,\ldots,9)$ from 2011 to 2019 to examine the net growth rate of the SFTS each year over a period of 9 years. The basic reproduction number is a metric of the pathogen's capacity to reproduce given the particular environmental conditions, and we include in the Appendix A the detailed procedure how the basic reproduction number is calculated for our model.

The calculated basic reproduction number per year from 2011 to 2019 is plotted in Fig. 5, where the blue, red, and yellow bars present distinct contributions of systemic transmission, co-feeding transmission, and transovarial transmission to the basic reproduction number. In Table 6, we also list the numerical values and percentages of the three transmission routes towards the reproduction numbers. The basic reproduction numbers varied slightly from year to year but consistently exceeded the threshold value to sustain the SFTS epidemic in the region during this period. In fact, we also considered these years from 2011 to 2019 as a single period and considered the model as a periodic system with 9 years as the period. We calculated the corresponding average basic reproduction number of model (2.1)-(2.5) as $R_{0-9Y}=1.2956$, and estimated the contribution of transo-

Table 6: The contributions of systemic transmission (ST), co-feeding transmission (CT), and transovarial transmission (TT), on the basic reproduction number $R_0^{(201i)}, i=1,2,\ldots,9$ from 2011 to 2019.

Year	Contribution of ST	Contribution of CT	Contribution of TT
2011	0.5676 (44.41%)	0.1410 (11.03%)	0.5694 (44.56%)
2012	0.5802 (43.69%)	0.1560 (11.75%)	0.5918 (44.56%)
2013	0.5501 (44.22%)	0.1420 (11.41%)	0.5519 (44.37%)
2014	0.5633 (43.80%)	0.1480 (11.51%)	0.5747 (44.69%)
2015	0.5617 (43.34%)	0.1511 (11.66%)	0.5833 (45.00%)
2016	0.5575 (44.44%)	0.1434 (11.43%)	0.5535 (44.13%)
2017	0.5582 (42.88%)	0.1538 (11.81%)	0.5898 (45.31%)
2018	0.5586 (43.11%)	0.1518 (11.71%)	0.5855 (45.18%)
2019	0.5624 (44.32%)	0.1470 (11.58%)	0.5596 (44.10%)

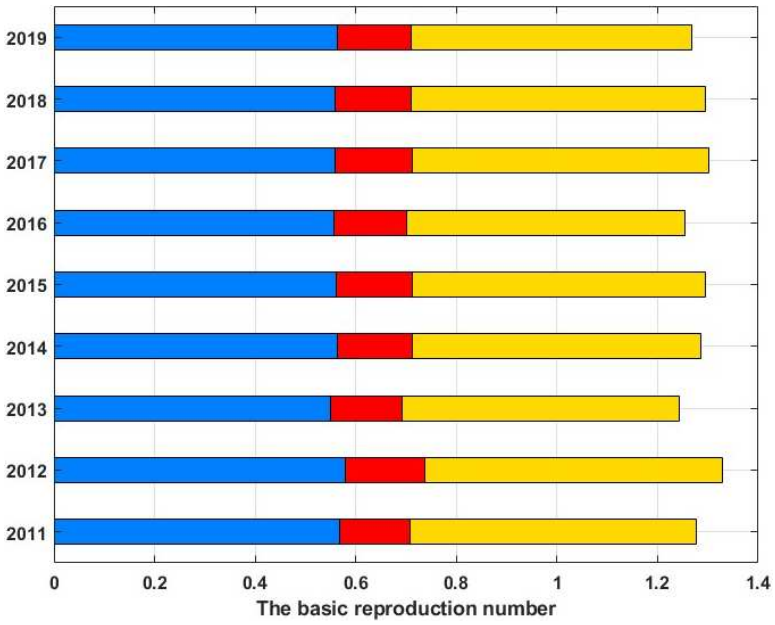

Figure 5: Bar chart of the basic reproduction numbers per year $R_0^{(201i)}$ from 2011 to 2019: the blue, red, and yellow bars represent the contributions of three transmission routes, systemic transmission, co-feeding transmission, and transovarial transmission, to the basic reproduction numbers $R_0^{(201i)}, i=1,2,\ldots,9$.

varial transmission to the basic reproduction number around 44.50%. This rather high contribution shows the importance of interventions in eradicating transovarial transmission.

Sensitivity Analysis: To inform the relative importance of plausible public health interventions, we used the method developed in [4] to perform a sensitivity analysis to evaluate the influence of some parameters on the average 9-year basic reproductive num-

Table 7: Sensitivity indices of the average 9-year basic reproduction number and the 9-year total estimated SFTS cases.

Parameter	Value	Sensitivity index of R_{0-9Y}	Sensitivity index of C_{SFTS}
θ	0.072	0.2002	0.5234
r_T	1071	0.2562	1.4946
c_n	0.335	0.1086	0.5769
c_a	0.449	0.0520	0.1115
$p_{RL}(p_{RN})$	0.5	0.8915	3.3652
p_{GA}	0.7	0.0459	0.2202
r_R	0.14	-0.1275	-0.4431
r_G	0.15	-0.0266	-0.1127
s	1.343	-0.6220	-2.8358

ber and the estimated 9-year total case of SFTS. The sensitivity analysis is presented in Table 7, which shows that the sensitivity indices of 9-year averaged basic reproduction number R_{0-9Y} and the 9-year total estimated SFTS case C_{SFTS} are negative with respect to r_R, r_G, s are negative, and positive with respect to $\theta, r_T, c_n, c_a, p_{RL}, p_{GA}$. Our sensitivity analysis shows that the probability of systemic transmission $p_{RL}(p_{RN})$ has a significant impact on both the average 9-year basic reproduction number and the estimated 9-year total SFTS cases.

Impact of Temperature: We considered further the influence of high temperature on SFTS transmission. 13.60°C is the lowest temperature at which egg-laying adult H. longicornis ticks produce eggs. Moreover, we observed the duration with a daily average temperature greater than 13.60°C as follows: 177 days in 2018 and an average of 171 days in other years. This shows that the longest duration with a daily average temperature greater than 13.60°C occurred in the year 2018. The higher temperature and longer duration (average daily temperature >13.60°C) in 2018 clearly facilitated the development and questing and feeding activities of H. longicornis at different stages (eggs, larvae, nymphs, and adults). Therefore, more ticks developed from the previous stage to the next in 2018.

The Roles of Adult Ticks: Fig. 6 presents the monthly densities of adult infected questing ticks (in the red curve) from 2011 to 2019 and the estimated cases of SFTS (in the gray curve) in the Dalian region. It is clear that the peak times of the two curves are not synchronized. The number of adult infected ticks peaked during each of the nine years 2011-2019 roughly in September or October, which was $1\sim2$ months later than the peak time of monthly SFTS cases in the same year. This shows that adult infected ticks contributed less to SFTS cases in the same year, but contributed significantly to the cases in the following year. For example, we observed that the abundance of A_{qi} in the year 2017 caused a rapid increase in SFTS cases in 2018. This adds another evidence for the significant role of transovarial transmission.

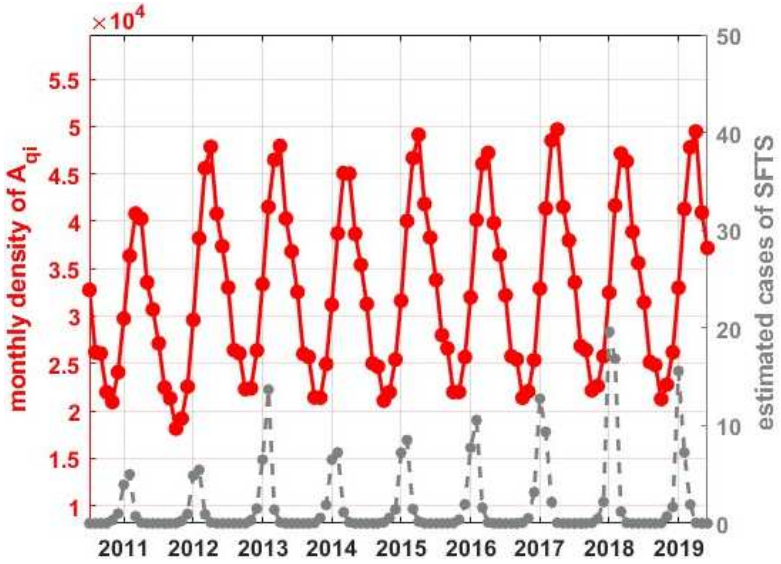

Figure 6: The densities of infected H. longicornis during 2011-2019. The light red curve is for infected questing nymphs; the dark red curve is for infected questing adult ticks.

5 Conclusion and discussion

We formulated a stage-dependent transmission dynamics model for the emerging tick-borne zoonotic disease SFTS, taking into consideration the coexisting systemic, co-feeding and transovarial transmission pathways. The model was fitted to the SFTS cases in the Dalian region during the period 2011 to 2019 and then validated using the surveillance data in the same region during the period 2020-2023.

The fitted model allowed us to estimate the average basic reproduction number $R_0 = 1.3$ for the transmission of the severe fever with thrombocytopenia syndrome virus in the tick-host system subject to the seasonal temperature variations in the region. This clearly shows that the disease has been established in the natural system, so SFTS will remain an endemic disease in human and animal populations and public health interventions must be planned to mitigate the disease burden.

The developed model also allowed us to quantify the contribution to the basic reproduction number and SFTS cases in the human population of the three distinct transmission pathways. Given the estimated contribution 44.50% to the basic reproduction number which is around 1.3, transovarial transmission has been playing a major role in the establishment of the virus in the tick-host system so any public health intervention to block this transmission pathway will be significant. This calls for the development of safe and effective vaccines to immunize the main host, goats, for adult ticks. More modeling studies motivated by emerging public health interventions are needed.

Our numerical study on the earlier arrival of the peak time of SFTS cases than the peak time of adult infected ticks, in conjunction with the high percentage of contribution of

transovarial transmission, provides insight into the importance of an appropriate public health message of a severe SFTS season after a year of production and infection of adult ticks due to a larger number of days with higher temperatures (13.60°C in the study region). A future study, based on our proposed model and incorporating the prediction of future temperatures under different climate change scenarios, can provide an assessment of the future risk of SFTS infection.

Appendix A.

Here, we provide a detailed procedure to calculate the basic reproduction number of the proposed model.

Let

$$u(t)=\big(E_i(t),L_{qi}(t),L_{fi}(t),N_{qi}(t),N_{fi}(t),A_{qi}(t),A_{fi}(t),A_{li}(t),R_i(t),G_i(t)\big)$$

be the vector which includes all infectious variables for system (2.1)-(2.5). Linearizing system (2.1)-(2.5) at the disease-free periodic solution

$$\big(E_s^*(t),0,L_{qs}^*(t),0,L_{fs}^*(t),0,N_{qs}^*(t),0,N_{fs}^*(t),0,A_{qs}^*(t),0,A_{fs}^*(t),0,A_{ls}^*(t),0,R_s^*(t),0,G_s^*(t),0\big),$$

we then produce the following system:

$$\frac{du(t)}{dt}=\big(F(t)-V(t)\big)u(t),$$

where

$$F(t)=\begin{pmatrix}F_1(t) & F_2(t)\\ F_3(t) & F_4(t)\end{pmatrix},\quad V(t)=\begin{pmatrix}V_1(t) & V_2(t)\\ V_3(t) & V_4(t)\end{pmatrix}$$

with

$$F_1(t)=\begin{pmatrix}0&0&0&0&0\\0&0&0&0&0\\0&0&0&\dfrac{\ln(1-c_n)^{-1}T_{fn}^N(t)\beta_{Nq}(t)\beta_{Lq}(t)L_{qs}^*(t)}{R_s^*(t)}&0\\0&0&0&0&0\\0&0&0&\dfrac{\ln(1-c_n)^{-1}T_{fn}^N(t)\beta_{Nq}^2(t)N_{qs}^*(t)}{R_s^*(t)}&0\end{pmatrix},$$

$$F_2(t)=\begin{pmatrix}0&0&0&0&0\\0&0&0&0&0\\0&0&0&\dfrac{p_{RL}\beta_{Lq}(t)L_{qs}^*(t)}{R_s^*(t)}&0\\0&0&0&0&0\\0&0&0&\dfrac{p_{RN}\beta_{Nq}(t)N_{qs}^*(t)}{R_s^*(t)}&0\end{pmatrix},$$

$$F_3(t)=\begin{pmatrix}0&0&0&0&0\\0&0&0&0&0\\0&0&0&0&0\\0&p_{LR}\beta_{Lq}(t)&0&p_{NR}\beta_{Nq}(t)&0\\0&0&0&0&0\end{pmatrix},$$

$$F_4(t)=\begin{pmatrix}0&0&0&0&0\\\dfrac{\ln(1-c_a)^{-1}T^A_{fa}(t)\beta^2_{Aq}(t)A^*_{qs}(t)}{G^*_s(t)}&0&0&0&\dfrac{p_{GA}\beta_{Aq}(t)A^*_{qs}(t)}{G^*_s(t)}\\0&0&0&0&0\\0&0&0&0&0\\p_{AG}\beta_{Aq}(t)&0&0&0&0\end{pmatrix},$$

$$V_1(t)=\begin{pmatrix}d_E(t)+\mu_E&0&0&0&0\\-d_E(t)&\beta_{Lq}(t)+\mu_{Lq}&0&0&0\\0&-\beta_{Lq}(t)&d_{Lf}(t)+\mu_{Lf}&0&0\\0&0&-d_{Lf}(t)&\beta_{Nq}(t)+\mu_{Nq}&0\\0&0&0&-\beta_{Nq}(t)&d_{Nf}(t)+\mu_{Nf}\end{pmatrix},$$

$$V_2(t)=\begin{pmatrix}0&0&-r_T d_{Legg}(t)\theta e^{-sd_{Legg}(t)A^*_{ls}(t)}&0&0\\0&0&0&0&0\\0&0&0&0&0\\0&0&0&0&0\\0&0&0&0&0\end{pmatrix},$$

$$V_3(t)=\begin{pmatrix}0&0&0&0&-d_{Nf}(t)\\0&0&0&0&0\\0&0&0&0&0\\0&0&0&0&0\\0&0&0&0&0\end{pmatrix},$$

$$V_4(t)=\begin{pmatrix}\beta_{Aq}(t)+\mu_{Aq}&0&0&0&0\\-\beta_{Aq}(t)&d_{Af}(t)+\mu_{Af}&0&0&0\\0&-\alpha_F d_{A_f}(t)&d_{Legg}(t)+\mu_{A_l}&0&0\\0&0&0&\mu_R&0\\0&0&0&0&\mu_G\end{pmatrix}.$$

Let $Y(t,s), t\geq s$, be the evolution operator of the linear periodic system $dy/dt=-V(t)y$. That is, for any $s\in\mathbb{R}$, the 10×10 matrix $Y(t,s)$ satisfies

$$\frac{dY(t,s)}{dt}=-V(t)Y(t,s),\quad \forall t\geq s,\quad Y(s,s)=I_{10},\tag{A.1}$$

where I_{10} is the 10×10 identity matrix. Let C_ω be the ordered Banach space of all ω-periodic functions from $\mathbb{R}^1$ to $\mathbb{R}^{10}$, equipped with the maximum norm. In the periodic envi-

ronment, we assume that $\psi(s)\in C_\omega$ represents the initial distribution of infected egg, larval, nymphal, and adult ticks with different behaviors, questing, feeding, and egg-laying. Then $F(s)\psi(s)$ characterizes the distribution of new infections caused by the initial infectious ticks and hosts who were introduced at time s. Given $t\geq s$, then $Y(t,s)F(s)\psi(s)$ denotes the distribution of infectious ticks and hosts who were newly infected at time s and remain infectious until time t. It follows that

$$\int_{-\infty}^{t} Y(t,s)F(s)\psi(s)ds=\int_{0}^{\infty} Y(t,t-a)F(t-a)\psi(t-a)da$$

represents the distribution of accumulative new infected ticks at time t produced by all those infected ticks $\psi(s)$ introduced at previous time to t. Then, we can define a linear operator $L:C_\omega\to C_\omega$ by

$$(L\psi)(t)=\int_{0}^{\infty} Y(t,t-a)F(t-a)\psi(t-a)da,\quad \forall t\in\mathbb{R},\quad \psi\in C_\omega.$$

Based on the next generation matrix method in [30], we denote L as the next population reproduction operator and define the net reproduction number as $\mathcal{R}_0:=\rho(L)$, the spectral radius of L.

Acknowledgments

This work was supported by the National Natural Science Foundation of China (Grant No. 12171074), by the Postgraduate Educational Reform program, PR China (Grant No. LNYJG2024086), and by the Natural Science Foundation of Liaoning, PR China (Grant No. 2024-MSBA-46).

References

[1] E. Bagnicka, E. Wallin, M. Łukaszewicz, and T. Ådnøy, *Heritability for reproduction traits in Polish and Norwegian populations of dairy goat*, Small Rumin. Res., 68(3):256–262, 2007.

[2] C. J. Bao et al., *A family cluster of infections by a newly recognized bunyavirus in eastern China, 2007: Further evidence of person-to-person transmission*, Clin. Infect. Dis., 53(12):1208–1214, 2011.

[3] F. Brauer and Z. Ma, *Stability of stage-structured population models*, J. Math. Anal. Appl., 126:301–315, 1987.

[4] N. Chitnis, J. M. Hyman, and J. M. Cushing, *Determining important parameters in the spread of malaria through the sensitivity analysis of a mathematical model*, Bull. Math. Biol., 70(5):1272–1296, 2008.

[5] B. Deng et al., *Meteorological factors and tick density affect the dynamics of SFTS in Jiangsu province, China*, PLoS Negl. Trop. Dis., 16(5):e0010432, 2022.

[6] K. Fujimoto and N. Yamaguti, *The effect of temperature on the oviposition and development of Haemaphysalis longicornis and H. flava (Acarina: Ixodidae)*, Jpn. J. Sanit. Zool., 38(3):225–232, 1987.

[7] H. Gaff and L. J. Gross, *Modeling tick-borne disease: A metapopulation model*, Bull. Math. Biol., 69:265–288, 2007.
[8] Z. Gai et al., *Person-to-person transmission of severe fever with thrombocytopenia syndrome bunyavirus through blood contact*, Clin. Infect. Dis., 54(2):249–252, 2012.
[9] H. Ge et al., *Impact of glycemia and insulin treatment in fatal outcome of severe fever with thrombocytopenia syndrome*, Int. J. Infect. Dis., 119:24–31, 2022.
[10] J. S. Gray, *The fecundity of Ixodes ricinus (L.) (Acarina: Ixodidae) and the mortality of its developmental stages under field conditions*, Bull. Ent. Res., 71:533–542, 1981.
[11] V. P. Guimarães, L. O. Tedeschi, and M. T. Rodrigues, *Development of a mathematical model to study the impacts of production and management policies on the herd dynamics and profitability of dairy goats*, Agric. Syst., 101:186–196, 2009.
[12] F. He, X. Zheng, and Z. Zhang, *Clinical features of severe fever with thrombocytopenia syndrome and analysis of risk factors for mortality*, BMC Infect. Dis., 21:1253, 2021.
[13] Z. He et al., *Severe fever with thrombocytopenia syndrome: A systematic review and meta-analysis of epidemiology, clinical signs, routine laboratory diagnosis, risk factors, and outcomes*, BMC Infect. Dis., 20:575, 2020.
[14] M.-D. Kim-Jeon et al., *Four-year surveillance of the vector hard ticks for SFTS in Ganghwa-do, Republic of Korea*, Korean J. Parasitol., 57(6):691–698, 2019.
[15] H. Li et al., *Epidemiological and clinical features of laboratory-diagnosed severe fever with thrombocytopenia syndrome in China, 2011–17: A prospective observational study*, Lancet Infect. Dis., 18(10):1127–1137, 2018.
[16] J. Z. Liu and Z. J. Jiang, *Studies on the bionomics of Haemaphysalis longicornis Neumann (Acari: Ixodidae) under laboratory conditions*, Acta Entomol. Sin., 41(3):280–283, 1998.
[17] Q. Liu, B. He, S. Huang, F. Wei, and X. Zhu, *Severe fever with thrombocytopenia syndrome, an emerging tick-borne zoonosis*, Lancet Infect. Dis., 14(8):763–772, 2014.
[18] Z. Lu et al., *Transmission of severe fever with thrombocytopenia syndrome virus by Haemaphysalis longicornis ticks, China*, Emerg. Infect. Dis., 24(5):868–871, 2018.
[19] L.-M. Luo et al., *Haemaphysalis longicornis ticks as reservoir and vector of severe fever with thrombocytopenia syndrome virus in China*, Emerg. Infect. Dis., 21:1770–1776, 2015.
[20] Z. Ma, *Mathematical Modelling and Analysis of Population Dynamics*, Anhui Science and Technology Press, 1996.
[21] K. Nah et al., *Assessing systemic and non-systemic transmission risk of tick-borne encephalitis virus in Hungary*, PLoS One, 14(6):e0217206, 2019.
[22] H. Oshima et al., *A patient with severe fever with thrombocytopenia syndrome (SFTS) infected from a sick dog with SFTS virus infection*, Jpn. J. Infect. Dis., 75(4):423–426, 2022.
[23] J. L. Perret, E. Guigoz, O. Rais, and L. Gern, *Influence of saturation deficit and temperature on Ixodes ricinus tick questing activity in a Lyme borreliosis-endemic area (Switzerland)*, Parasitol. Res., 86(6):554–557, 2000.
[24] S. Qi, W. Pang, J. Xing, Y. Liang, Y. Zhou, L. Kong, and S. Jin, *Epidemiological characteristics and spatial aggregation of severe fever with thrombocytopenia syndrome (SFTS) in Dalian city from 2011 to 2023*, Chin. J. Public Health, 40(9):1052–1058, 2024.
[25] L. Qviller, L. Grøva, H. Viljugrein, I. Klingen, and A. Mysterud, *Temporal pattern of questing tick Ixodes ricinus density at differing elevations in the coastal region of western Norway*, Parasites Vectors, 7:179, 2014.
[26] R. Rosà, A. Pugliese, R. Norman, and P. J. Hudson, *Thresholds for disease persistence in models for tick-borne infections including non-viraemic transmission, extended feeding and tick aggregation*, J. Theor. Biol., 224:359–376, 2003.

[27] B. L. Schappach, R. K. Krell, V. L. Hornbostel, and N. P. Connally, *Exotic Haemaphysalis longicornis (Acari: Ixodidae) in the United States: Biology, ecology, and strategies for management*, J. Integr. Pest Manag., 11(1):21, 2020.
[28] R. T. Trout Fryxell, T. Chavez-Lindell, R. A. Butler, and A. Odoi, *Environmental variables serve as predictors of the invasive Asian longhorned tick (Haemaphysalis longicornis Neumann): An approach for targeted tick surveillance*, PLoS One, 18(11):e0292595, 2023.
[29] D. M. Tufts, L. B. Goodman, M. C. Benedict, A. D. Davis, M. C. VanAcker, and M. Diuk-Wasser, *Association of the invasive Haemaphysalis longicornis tick with vertebrate hosts, other native tick vectors, and tick-borne pathogens in New York City, USA*, Int. J. Parasitol., 51(2):149–157, 2021.
[30] W. Wang and X. Q. Zhao, *Threshold dynamics for compartmental epidemic models in periodic environments*, J. Dynam. Differential Equations, 20(3):699–717, 2008.
[31] Z. Wang et al., *Development and comparison of time series models in predicting severe fever with thrombocytopenia syndrome cases – Hubei Province, China, 2013–2020*, China CDC Weekly, 6(37):962–967, 2024.
[32] J. Wu and X. Zhang, *Transmission Dynamics of Tick-Borne Diseases with Co-Feeding, Developmental and Behavioural Diapause*, Springer Nature, 2020.
[33] B. Xu et al., *Metagenomic analysis of fever, thrombocytopenia and leukopenia syndrome (FTLS) in Henan Province, China: Discovery of a new bunyavirus*, PLoS Pathog., 7(11):e1002369, 2011.
[34] K. Yamaji, H. Aonuma, and H. Kanuka, *Distribution of tick-borne diseases in Japan: Past patterns and implications for the future*, J. Infect. Chemother., 24(6):499–504, 2018.
[35] S. Yan and X. Zhang, *Dynamics of a tick-borne disease model with birth pulse and pesticide pulse at different moments*, J. Nonl. Mod. Anal., 7:111–134, 2025.
[36] Y. Yano, S. Shiraishi, and T. Uchida, *Effects of temperature on development and growth in the tick, Haemaphysalis longicornis*, Exp. Appl. Acarol., 3:73–78, 1987.
[37] Y. Yano, S. Shiraishi, and T. Uchida, *Effects of humidity on development and growth in the tick, Haemaphysalis longicornis*, J. Fac. Agric. Kyushu Univ., 32(3/4):141–146, 1988.
[38] X. J. Yu et al., *Fever with thrombocytopenia associated with a novel bunyavirus in China*, N. Engl. J. Med., 364(16): 1523–1532, 2011.